AD-A067 992 CORNELL UNIV ITHACA N Y DEPT OF MATERIALS SCIENCE A--ETC F/G 11/6
TEMPERATURE DEPENDENCE OF THE FLOW STRESS AND DUCTILITY OF ANNE--ETC(U)
OCT 77 D J KRENITSKY, D G AST N00014-77-C-0546
UNCLASSIFIED TR-2 NL

| OF |
AD
A067992

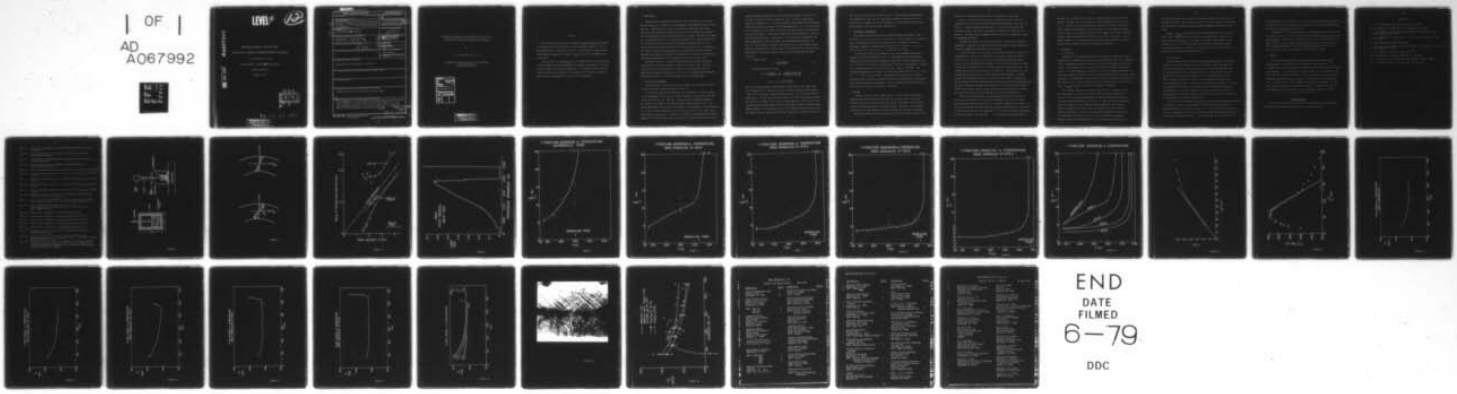

END
DATE
FILMED
6-79
DDC

TEMPERATURE DEPENDENCE OF THE FLOW STRESS AND DUCTILITY OF ANNEALED & UNANNEALED AMORPHOUS $Fe_{40}Ni_{40}P_{14}B_6$

D.J. Krenitsky, D.G. Ast

Contract Number: NR039-151/N00014-77-C-0546

Technical Report #2

October 1977

UNCLASSIFIED

SECURITY CLASSIFICATION OF THIS PAGE (When Data Entered)

REPORT DOCUMENTATION PAGE

READ INSTRUCTIONS BEFORE COMPLETING FORM

1. REPORT NUMBER: Technical Report No. 2
2. GOVT ACCESSION NO.:
3. RECIPIENT'S CATALOG NUMBER: (9)
4. TITLE (and Subtitle): (6) Temperature Dependence of the Flow Stress and Ductility of Annealed and Unannealed Amorphous $Fe_{40}Ni_{40}P_{14}B_6$
5. TYPE OF REPORT & PERIOD COVERED: Technical Progress Report
6. PERFORMING ORG. REPORT NUMBER:
7. AUTHOR(s): (10) D.J. Krenitsky [redacted] D.G. Ast
8. CONTRACT OR GRANT NUMBER(s): (14) TR-2
9. PERFORMING ORGANIZATION NAME AND ADDRESS: Materials Sci. & Eng.; Bard Hall, Cornell Univ. ; Ithaca, NY 14853
10. PROGRAM ELEMENT, PROJECT, TASK AREA & WORK UNIT NUMBERS: (15) N00014-77-C-0546, NRO 39-151
11. CONTROLLING OFFICE NAME AND ADDRESS: (12) 36p.
12. REPORT DATE: (11) Oct 77
13. NUMBER OF PAGES: 29
14. MONITORING AGENCY NAME & ADDRESS (if different from Controlling Office):
15. SECURITY CLASS. (of this report): Unclassified
15a. DECLASSIFICATION/DOWNGRADING SCHEDULE:
16. DISTRIBUTION STATEMENT (of this Report): Distribution of this document is unlimited
17. DISTRIBUTION STATEMENT (of the abstract entered in Block 20, if different from Report):
18. SUPPLEMENTARY NOTES:
19. KEY WORDS (Continue on reverse side if necessary and identify by block number): Metallic glass, Flow stress, Ductility, Embrittlement.
20. ABSTRACT (Continue on reverse side if necessary and identify by block number): The flow stress of the Fe-Ni based glass $Fe_{40}Ni_{40}P_{14}B_6$ was measured between 78 and 600°K using a novel technique based on the compression of ring shaped specimen. The flow stress at RT was 320,000 psi and increased with decreasing temperature. The effect of annealing is to shift the ductile to brittle transition temperature to T_{anneal} ANNEALING TEMPERATURE.

403 152

DD FORM 1 JAN 73 1473 EDITION OF 1 NOV 65 IS OBSOLETE
S/N 0102-LF-014-6601

Unclassified
SECURITY CLASSIFICATION OF THIS PAGE (When Data Entered)

Temperature Dependence of the Flow Stress and Ductility of Annealed and Unannealed Amorphous $Fe_{40}Ni_{40}P_{14}B_6$

by

D. J. Krenitsky and D. G. Ast

Department of Materials Science and Engineering
Cornell University
Ithaca, New York 14853

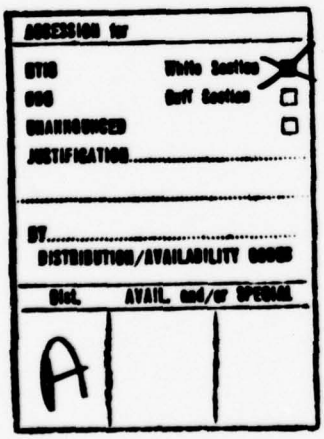

Abstract

The flow stress and ductility of amorphous $Fe_{40}Ni_{40}P_{14}B_6$ was investigated on as-prepared and annealed ribbons over the temperature range 78 - 573 K. The embrittlement is characterized by a rise in the ductile to brittle transition temperature T_{dtb}, such that $T_{dtb} \simeq T_{anneal}$ and sets in at temperatures as low as 423 K.

The flow stress of $Fe_{40}Ni_{40}P_{14}B_6$ at room temperature is 2.21 GPa (320 KSI), in good agreement with the extrapolation from hardness measurements. The flow stress increases with decreasing temperature. The increase can be accounted for in dislocation based models of the deformation of a metallic glass but is more difficult to understand in terms of a free volume model.

1. INTRODUCTION

Knowledge of the temperature dependence of the flow stress, σ_y, of Fe base metallic glasses is of interest in the development of deformation models for these materials. Unfortunately, no direct measurements are available, since these metallic glasses can only be prepared in the form of thin ribbons which fracture in a macroscopically brittle fashion when tested in tension. The fracture strength, σ_f, of a brittle material is not necessarily identical to σ_y, because failure may be controlled by the stress neccessary to propagate existing defects, such as cracks, rather than being determined by the intrinsic properties of the material. The fracture strength of $Fe_{40}Ni_{40}P_{14}B_6$, even if measured on carefully prepared specimens with reduced cross-sections, consistently lies below the value expected from hardness measurements, which indicates that in this alloy $\sigma_f < \sigma_y$(1).

This paper presents a technique for measuring the flow stress of metallic glasses which avoids the instability problems of the tensile test. The result obtained for the room temperature flow stress is in good agreement with the prediction from hardness measurements. The flow stress increases with decreasing temperature, and at 78 K is about 25% higher than at room temperature.

2. PRINCIPLE OF MEASUREMENT

The flow stress is measured by coiling the ribbon into a ring which is then compressed between two parallel platens (see Fig. 1).

At the initial stage of the compression, the deformation is entirely elastic and the longitudinal stress, σ_{yy}, is a linear function of the distance z from the neutral axis (see Fig. 2a). When σ_{yy} reaches σ_y, plastic deformation begins at the surface of the ribbon in the form of densely spaced shear bands which, upon further deformation, spread towards the interior. The deformation is self-arresting, i.e., stable, even in the absence of work hardening, since the shear bands cannot proceed past the neutral axis. Because of the absence of work hardening in metallic glasses (2), the shear bands fix the stress level at σ_y and the stress level in the

material closely approximates that of an ideal elastic-plastic solid (Fig. 2b). In order to extract σ_y from the compression test, one needs to know how the tensile test variables, i.e., the force F applied to the platens and the distance between the platens, are related to the bending parameters, i.e., the local radius R at the apex, and l, the length of the lever arm with which the restoring moment M acts on the platens. In the elastic range, the relation between R, l and ξ can be found using the theory of elastica (3). Since we are also interested in the mixed elastic-plastic case, the relation was experimentally determined (see Fig. 3). Over the range of interest, the relation can, in a satisfactory approximation, be represented by a linear relation. This leads to the following simple predictions for the relation between the force on the platens and the platen separation.

a) Elastic range:

$$F = \frac{2\, w\, E\, d^3\, K}{3(1 - \nu^2)\xi^2} \tag{1}$$

b) Mixed elastic-plastic range:

$$F \cdot \xi = \frac{\sigma_y\, d^2\, w}{2 \cdot (.653)(1 - \nu^2)} - \frac{2(.422)^2\, K\, w\, \sigma_y{}^3\, \xi^2}{3(.653)\, E^2\, (1 - \nu^2)} \tag{2}$$

$$K = 1 - \nu^2 + \nu \sqrt{(1 - \nu^2)/3}$$

where E is Young's modulus, d the thickness of the ribbon, w the ribbon width, and ν Poisson's ratio. Equations (1) and (2) predict a linear relation between F and $1/\xi^2$ in the elastic range and between $F \cdot \xi$ and ξ^2 in the mixed elastic-plastic case. If E and ν are known the slope of F vs $1/\xi^2$ of the elastic solution can be used to determine d, the effective ribbon thickness. This quantity varies somewhat along the ribbon and is, because of the uneven surface, not easily determined otherwise. The flow stress, σ_y, can then be found by either noting the onset of deviation from the predicted linear elastic behavior, or from the intercept or

the slope of the mixed elastic-plastic behavior. (The latter two determinations are independent of each other, and experimental agreement between the two is a sensitive test of whether or not the assumption of an ideal elastic-plastic solid can be applied to the material under investigation.)

3. EXPERIMENTAL ARRANGEMENTS

The material was obtained from Allied Chemical (Trade name Metglas ^{R} 2826) in the form of a continous thin ribbon of $\sim$2 mm width and .05 mm thickness. For compression tests, the material was coiled into single loops of 1 cm diameter, which were spotwelded. Annealing treatments were carried out, for a period of 1 hour, in a vacuum furnace with a base pressure of $\sim 1.3 \times 10^{-2}$ Pa ($\sim 10^{-5}$ Torr).

The rings were loaded into a parallel platen test arrangement fabricated of Cu, which is depicted schematically in Fig. 1. This apparatus was lowered into a stainless steel and brass dewar arrangement filled with a suitable temperature bath (LN_2, n-pentane, silicone oil) and inserted into an Instron testing machine. Compression of the platens was carried out at a crosshead speed of .508 cm/min. The corresponding maximum strain rates in the ribbon are $\sim 2 \times 10^{-2}$ sec^{-1} for $1/\xi = 3$ cm^{-1} and ~ 2 sec^{-1} for $1/\xi = 30$ cm^{-1}. Data analysis according to Eq. (1) and (2) was carried out by replotting the data with the help of a Data General Nova equipped with a Tektronix graphic copy terminal. Slopes and intercepts were determined by a least squares fit over the linear parts of the plot.

4. RESULTS

A typical result of a run is shown in Fig. 4. As the ring is increasingly compressed the load increases rapidly until first one side of the ring breaks, followed by the other, causing a step-like fall off. Eventually, the top platen contacts the bottom, and the load increases rapidly. The onset of this increase, corrected for the ribbon thickness, gives the position of zero platen separation.

The platen separation at which fracture occurs is a qualitative measure of the

ductility of the material and was therefore investigated in some detail.

Figures 5 to 9 show the inverse platen separation at failure versus test temperature for both as-received material and material annealed at 423, 473, 523 and 573 K. Figure 10 summarizes the results. It can be seen that annealing treatments as low as 423 K have a pronounced influence on the ductility of the material. The embrittlement disappears rapidly when the test temperature exceeds the annealing temperature.

In unannealed samples, the ductility decreases noticeably with decreasing temperature. Annealing, by sharply lowering the ductility at higher temperature, reduces the temperature dependence of the ductility.

In order to extract the flow stress, the deformation data were replotted as indicated by Eq. (1) and (2). The results for the data of Fig. 4 are shown in Fig. 11 and 12. From Fig. 11 it can be seen that deviation from the elastic solution occurs very gradually, which makes it difficult to determine σ_y reliably in this way. We therefore chose to determine σ_y from a least squares fit of the straight portion of the elastic-plastic plot (Fig. 12). The deviations from the straight line at large values of ξ^2 are caused by elastic behavior. At small values of ξ^2 the deviations are due to "kinking" of the ribbon. In general, σ_y values determined from the intercept agreed within 10% with σ_y values determined from the slope. Since the intercept method contains d^2, we consider the slope method somewhat more reliable and all values reported here were derived in this manner. The values for E and ν used in the analysis were 145 GPa (21 MPSI) and .4.

For both as-received material and material annealed at 423, 473, 523 and 573 K, σ_y was determined as a function of temperature. The results of these measurements are depicted in Fig. 13 to 17. Figure 18 summarizes the results. It can be seen that both unannealed and mildly annealed material exhibit a pronounced increase in flow stress at low temperature. At 78 K, the flow stress exceeds σ_y(RT) by about one quarter. This increase, is not observed in heavily annealed

material due to difficulties in obtaining a measurably long region of plastic behavior. In this case it is difficult to reliably determine the slope of $F \cdot \xi$ vs. ξ^2. From Fig. 12 can be seen that any inadvertent inclusion of the elastic portion lowers the slope and thus the flow stress. For this reason we believe that the absence of a pronounced increase at low temperatures in heavily annealed material reflects experimental difficulties, rather than a real effect. The apparent increase in σ_y at temperatures near the annealing temperature is also an artifact and is caused by the onset of homogeneous relaxation.

5. DISCUSSION

a) Ductility

Examination of the specimens shows that shear bands are formed at all test temperatures, in unannealed as well as in annealed specimens (Fig. 19). In addition to this inhomogeneous deformation process, a homogeneous deformation process also occurs. The contribution of the latter to the overall deformation is very small except if the test temperature is close to, or above the annealing temperature. In this case, homogeneous relaxation occurs at times comparable to the time scale of the experiment. The homogeneous process has been studied in more detail and will not be discussed here (4). There are indications that the rapid increase in ductility at $T_{test} \simeq T_{anneal}$ may not be solely due to homogeneous relaxation.

This evidence comes from conventional tensile tests on straight specimens which were pulled to fracture in an Instron testing machine equipped with a furnace. Prior to testing the specimens were annealed in situ for ten hours at selected temperatures between 423 and 573 K. These anneals were carried out under small loads in order to maintain specimen alignment. Such annealing results in specimens that shatter into many fragments when tested below the annealing temperature. However, when the annealed specimens are tested without lowering the temeprature, these fail in the same manner as unannealed specimens tested at room temperature. That is, the specimens fracture at one

point and the elastic recoil deforms the specimens (when viewed edge on) into an accordian like shape. This deformation results from the production of shear bands and occurs much too rapidly for any significant homogeneous deformation to take place.

At $T_{test} \simeq T_{anneal}$ even so-called embrittled specimens are ductile in the usual sense. Phenomenologically, the effect of annealing can be described as a shift in T_{dtb} towards T_{anneal}. This shift is noticeable after anneals at temperatures as low as 423 K and corresponds to the onset of exothermic activity in DSC experiments and to the onset of clustering as observed in TEM studies of specimens first thinned and then annealed (9).

b) Flow Stress

The room temperature flow stress of $Fe_{40}Ni_{40}P_{14}B_6$ determined in this investigation is 2.21 GPa (320 KSI) and, within the accuracy of the experiment, not influenced by annealing. The above value for σ_y is considerably higher than the reported yield stress by the manufacturer of 1.72 GPa (250 KSI) (5), and higher than the highest yield strength of 2.07 GPa (300 KSI) which we were able to measure in tension on a series of test specimens with reduced cross-sections and polished edges. The value of σ_y reported here, however, is in reasonable agreement with the value of 2.29 GPa (332 KSI) estimated from hardness measurements (1). We believe therefore that in most cases tensile failure of $Fe_{40}Ni_{40}P_{14}B_6$ is controlled by existing flaws and that the fracture strength does not represent the flow stress of the material.

The flow stress of amorphous $Fe_{40}Ni_{40}P_{14}B_6$ increases with decreasing temperature. The behavior is similar to that observed in crystalline materials where it is usually ascribed to an increase in Peierls stress. Thus the observed increase in σ_y at low temperatures can easily be accommodated by any deformation model which uses the movement of dislocations (6,7). It is more difficult to incorporate the ob-

served increase into the framework of free volume models which predict essentially a constant value of σ_y for temperatures below the glass transition temperature T_g (8) which in $Fe_{40}Ni_{40}P_{14}B_6$ is 643 K (9).

A comparable rise in fracture strength at low temperatures has been observed by Pampillo et al. (10) in Fe based alloys of the composition $Ni_{49}Fe_{29}P_{14}B_6Al_2$ and $Fe_{76}P_{16}C_4Si_2Al_2$. These results, together with the flow stress reported here, are shown in Fig. 20. These authors have argued that the rise in fracture strength with decreasing temperature (except for $Fe_{76}P_{16}C_4Si_2Al_2$ below 200 K) reflects a rise of the flow stress. Our observations corroborate this claim.

6. SUMMARY

The flow stress and ductility of as-received and of annealed amorphous $Fe_{40}Ni_{40}P_{14}B_6$ was investigated over the temperature range between 78 - 573 K by compressing loops of the material and assuming an ideal elastic-plastic behavior in the analysis. It was found that the embrittlement sets in at temperatures as low as 423 K and is best described as a rise in the ductile to brittle transition temperature T_{dtb} such that $T_{dtb} \approx T_{anneal}$. The flow stress of $Fe_{40}Ni_{40}P_{16}B_6$ at RT is 2.21 GPa (320 KSI) in good agreement with hardness measurements. The flow stress increases with decreasing temperatures which is compatible with what one would expect from dislocation models for the deformation of metallic glasses.

Acknowledgements

This research was sponsored by the Office of Naval Research (NR039-151/N0014-77-C-0546) and the Materials Science Center at Cornell University.

References

1. L. E. Tanner and R. Ray, Scripta Met., 11, 783 (1977).

2. T. Masumoto and R. Maddin, Mat. Sci. and Engr., 19, 1 (1975).

3. R. V. Southwell, "An Introduction to the Theory of Elasticity", Dover Publications Inc., New York.

4. T. D. Hadnagy, D. J. Krenitsky, D. G. Ast and C. Y. Li, Scripta Met. 12, 45 (1978).

5. Allied Chemical Preliminary Data Sheet.

6. J. C. M. Li, in "Frontiers in Materials Science", (L. E. Murr and C. Stein, eds.) Marcel Dekker, NY (1976).

7. J. J. Gilman, J. Appl. Phys., 46, 1625 (1975).

8. F. Spaepen and D. Turnbull, Scripta Met., 8, 563 (1974).

9. D. G. Ast and D. J. Krenitsky, Mat. Sci. and Engr., 23, 241 (1976).

10. C. A. Pampillo and D. F. Polk, Acta Met. 22, 741 (1974).

Fig. 1: Experimental arrangement used for measuring flow stress as a function of temperature.

Fig. 2: Stress distribution in the ribbon for the elastic (a) and mixed elastic-plastic case (b).

Fig. 3: Relation between platen separation and radius of curvature at apex of ribbon under test.

Fig. 4: Load on platen vs platen separation for a specimen annealed at 473 K and tested at 400 K.

Fig. 5: Reciprocal fracture separation vs. temperature for unannealed $Fe_{40}Ni_{40}P_{14}B_6$.

Fig. 6: Reciprocal fracture separation vs. temperature for $Fe_{40}Ni_{40}P_{14}B_6$ annealed at 423 K.

Fig. 7: Reciprocal fracture separation vs. temperature for $Fe_{40}Ni_{40}P_{14}B_6$ annealed at 473 K.

Fig. 8: Reciprocal fracture separation vs. temperature for $Fe_{40}Ni_{40}P_{14}B_6$ annealed at 523 K.

Fig. 9: Reciprocal fracture separation vs. temperature for $Fe_{40}Ni_{40}P_{14}B_6$ annealed at 573 K.

Fig. 10: Summarized results for the influence of annealing on inverse fracture separation of amorphous $Fe_{40}Ni_{40}P_{14}B_6$.

Fig. 11: Force on platen (F) versus square of inverse platen separation ($1/\xi^2$) for a specimen annealed at 473 K and tested at 400 K (data of Fig. 4).

Fig. 12: Force on platen times platen separation vs. squared platen separation for a specimen annealed at 473 K and tested at 400 K. (Data of Fig. 4).

Fig. 13: Flow stress vs. temperature for unannealed $Fe_{40}Ni_{40}P_{14}B_6$.

Fig. 14: Flow stress vs. temperature for $Fe_{40}Ni_{40}P_{14}B_6$ annealed at 423 K.

Fig. 15: Flow stress vs. temperature for $Fe_{40}Ni_{40}P_{14}B_6$ annealed at 473 K.

Fig. 16: Flow stress vs. temperature for $Fe_{40}Ni_{40}P_{14}B_6$ annealed at 523 K.

Fig. 17: Flow stress vs. temperature for $Fe_{40}Ni_{40}P_{14}B_6$ annealed at 573 K.

Fig. 18: Summarized results for the influence of annealing on flow stress of amorphous $Fe_{40}Ni_{40}P_{14}B_6$.

Fig. 19: Shear bands formed by bending. The visibility of the bands has been enhanced by etching. The view is as in Fig. 2. The ribbon thickness (vertical dimension) is $\sim$60μm.

Fig. 20: Comparison between the temperature dependence of the fracture strength of $Ni_{49}Fe_{29}P_{14}B_6Al_2$ and $Fe_{76}P_{16}C_4Si_2Al_2$ as reported by Pampillo and Polk and the temperature dependence of the flow stress of $Fe_{40}Ni_{40}P_{14}B_6$ as measured in this investigation.

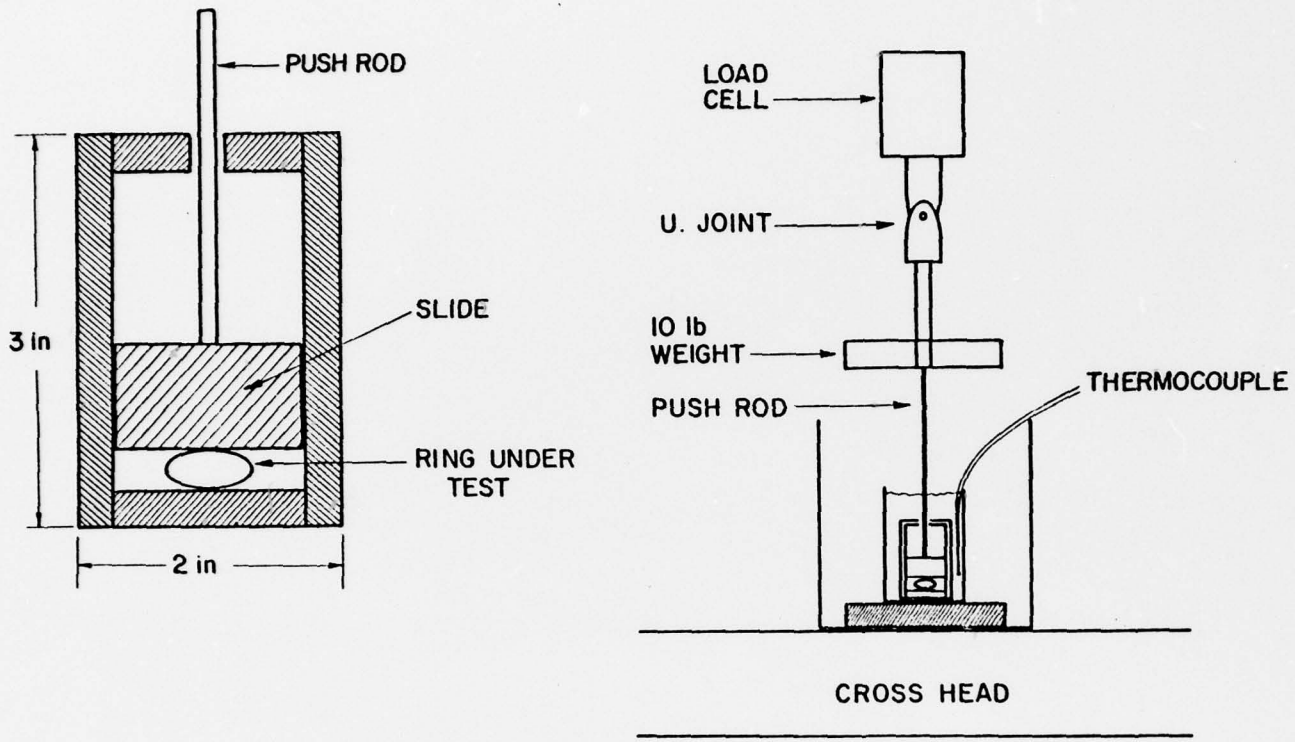
PUSH ROD
3 in
SLIDE
RING UNDER TEST
2 in
LOAD CELL
U. JOINT
10 lb WEIGHT
PUSH ROD
THERMOCOUPLE
CROSS HEAD

FIGURE 1

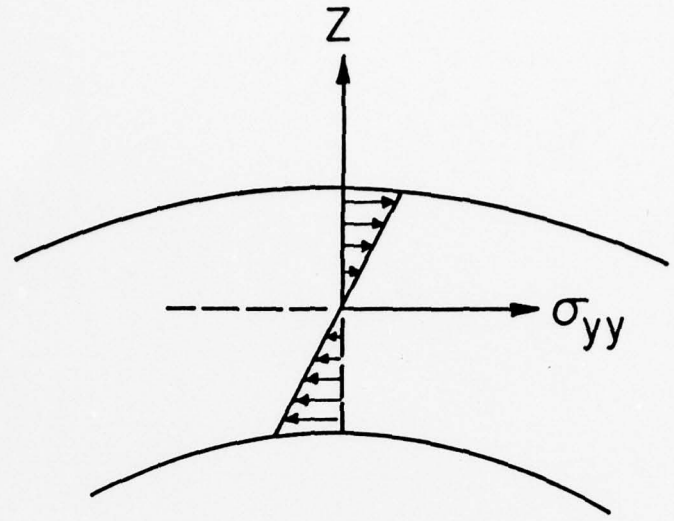

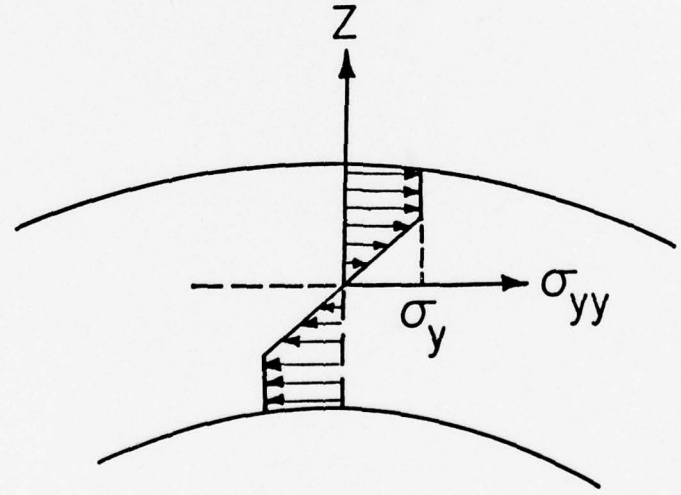

FIGURE 2

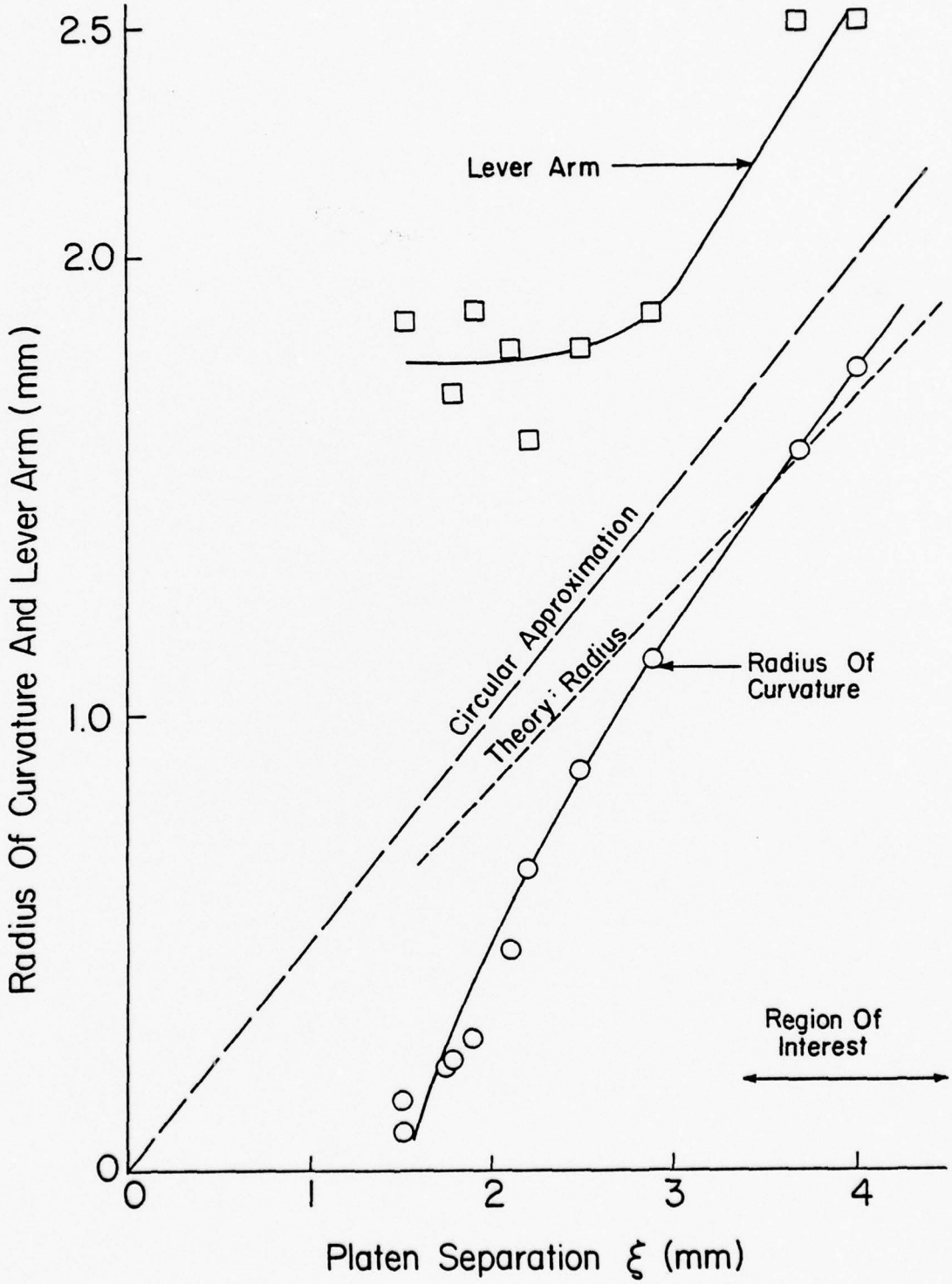
2.5
2.0
1.0
0
Lever Arm
Circular Approximation
Theory: Radius
Radius Of Curvature
Region Of Interest
0
1
2
3
4
Radius Of Curvature And Lever Arm (mm)
Platen Separation ξ (mm)

FIGURE 3

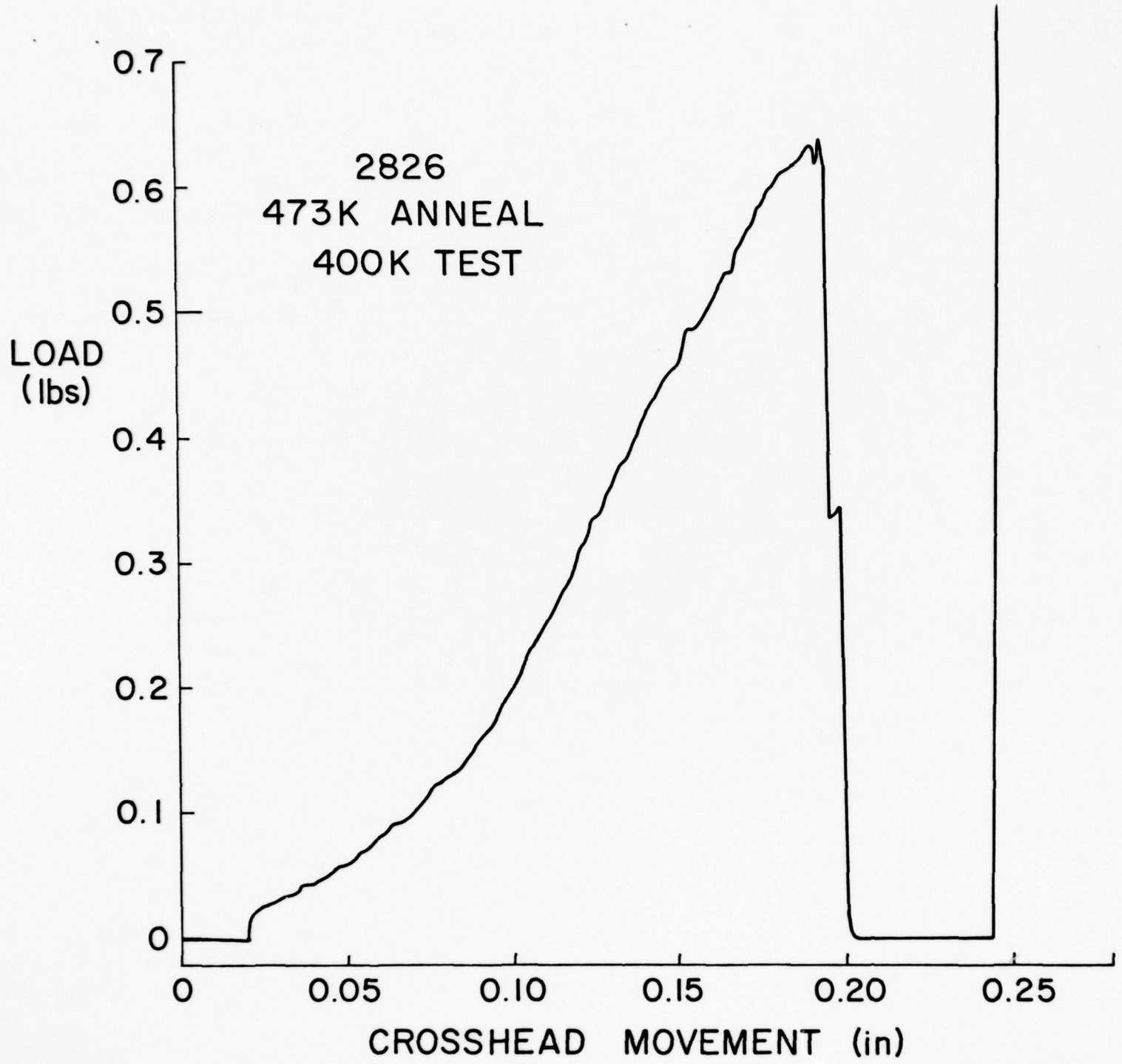
2826
473K ANNEAL
400K TEST
LOAD
(lbs)
0.7
0.6
0.5
0.4
0.3
0.2
0.1
0
0
0.05
0.10
0.15
0.20
0.25
CROSSHEAD MOVEMENT (in)

FIGURE 4

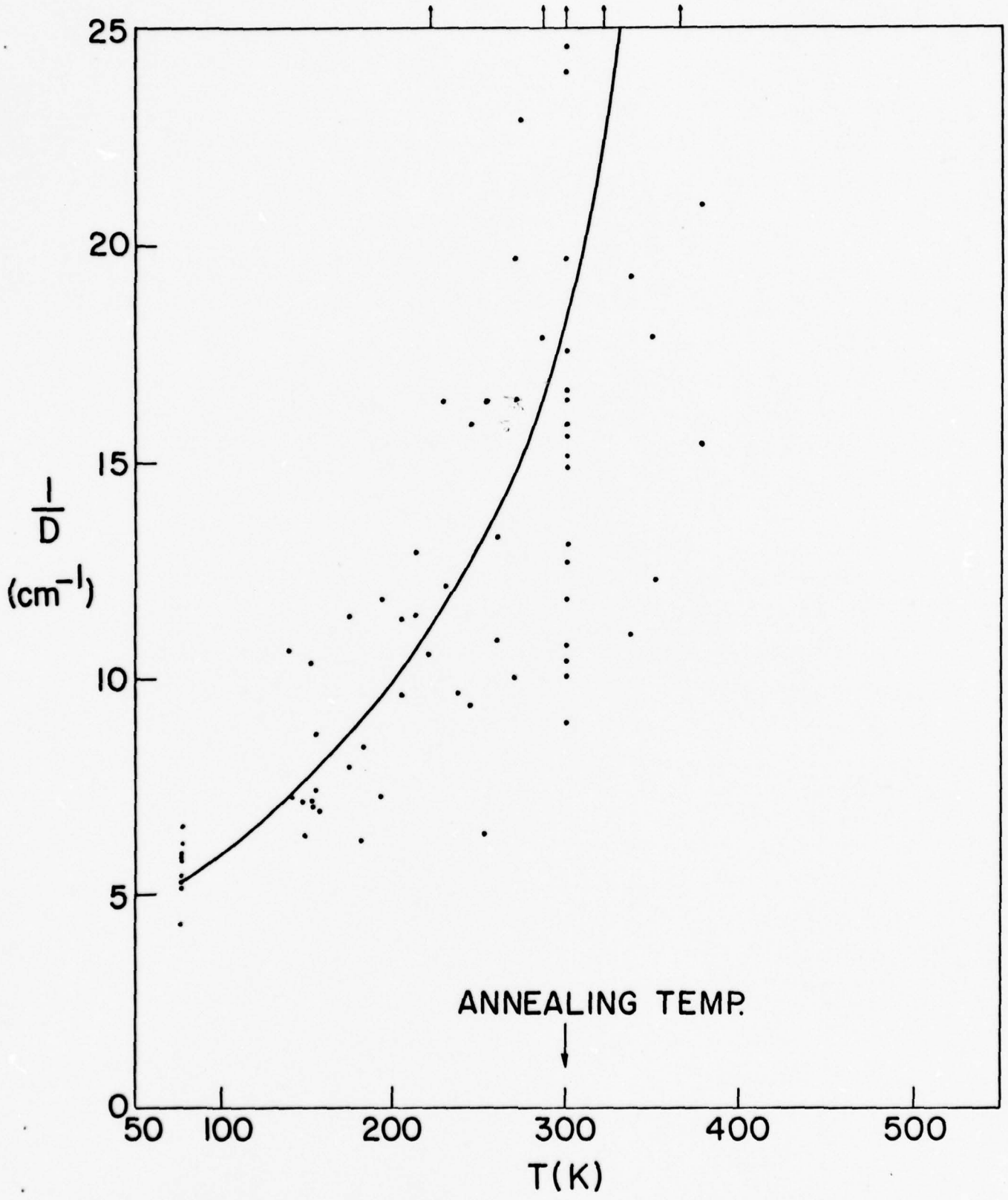
1/ FRACTURE SEPARATION vs TEMPERATURE
UNANNEALED 2826
25
20
15
10
5
0
1/D
(cm⁻¹)
ANNEALING TEMP.
50
100
200
300
400
500
T(K)

FIGURE 5

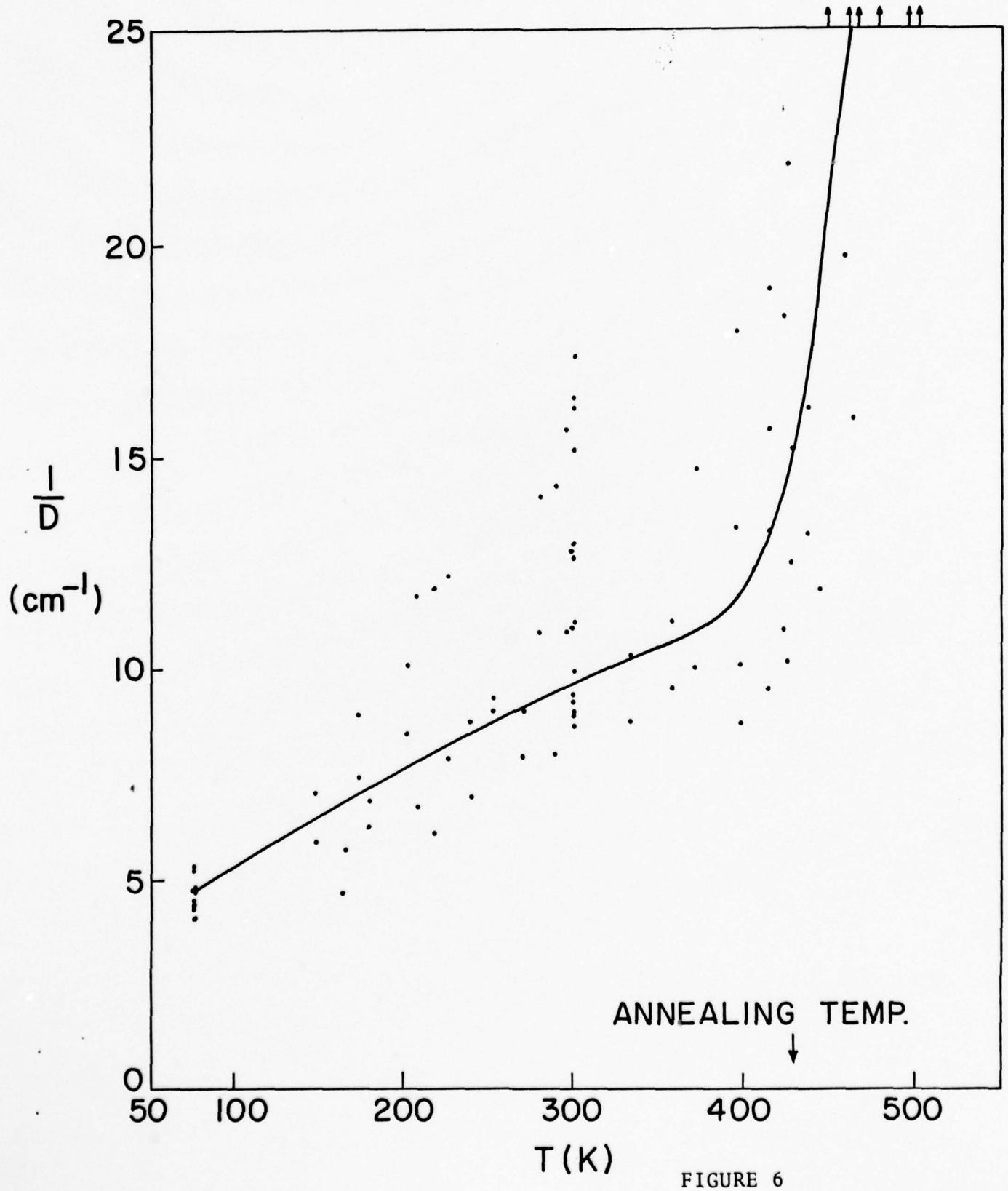
1/FRACTURE SEPARATION vs TEMPERATURE
2826 ANNEALED AT 423 K
25
20
15
10
5
0
1/D
(cm⁻¹)
ANNEALING TEMP.
50
100
200
300
400
500
T(K)

FIGURE 6

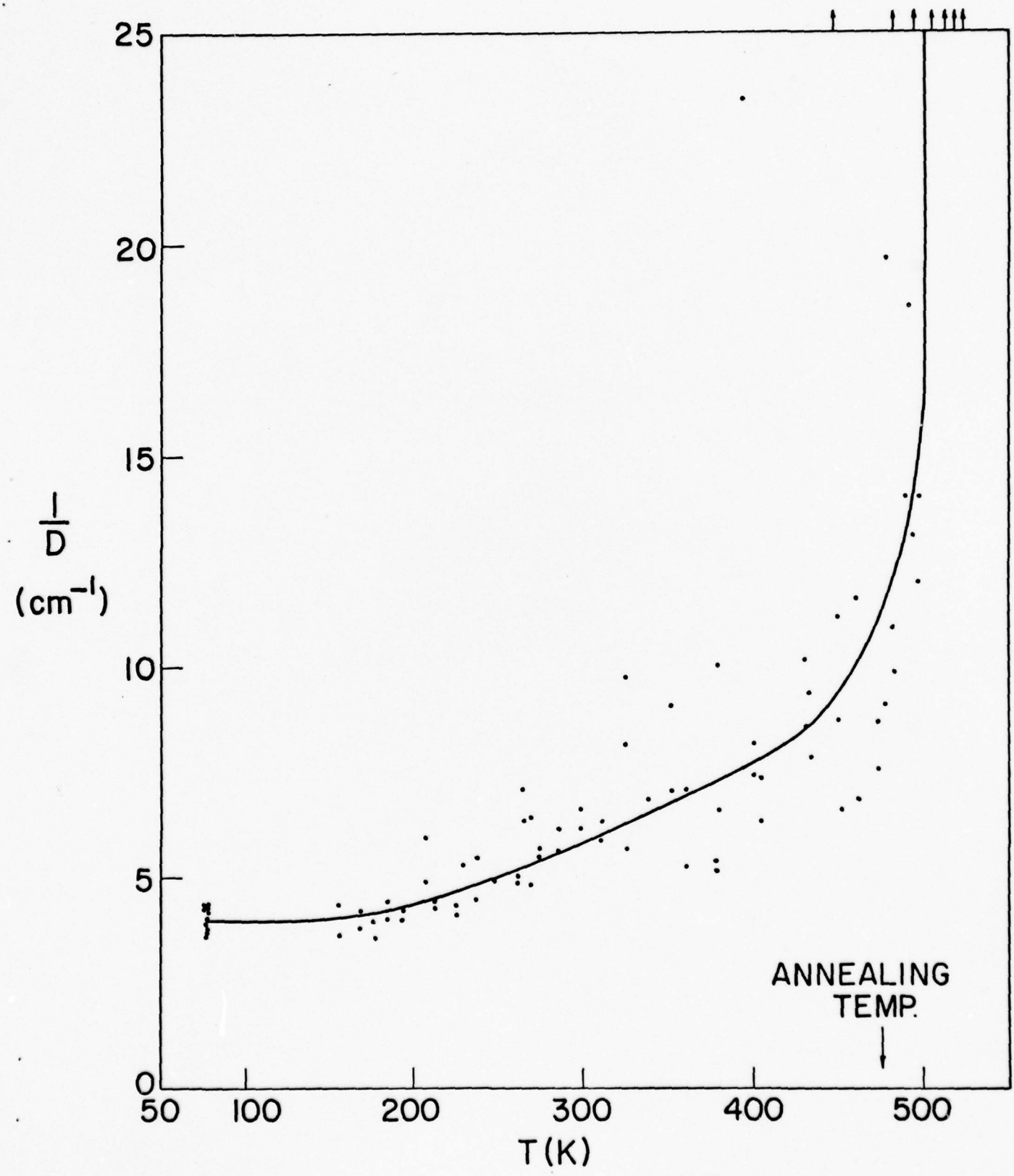
1/ FRACTURE SEPARATION vs TEMPERATURE
2826 ANNEALED AT 473 K
25
20
15
10
5
0
1/D
(cm⁻¹)
50
100
200
300
400
500
T(K)
ANNEALING
TEMP.

FIGURE 7

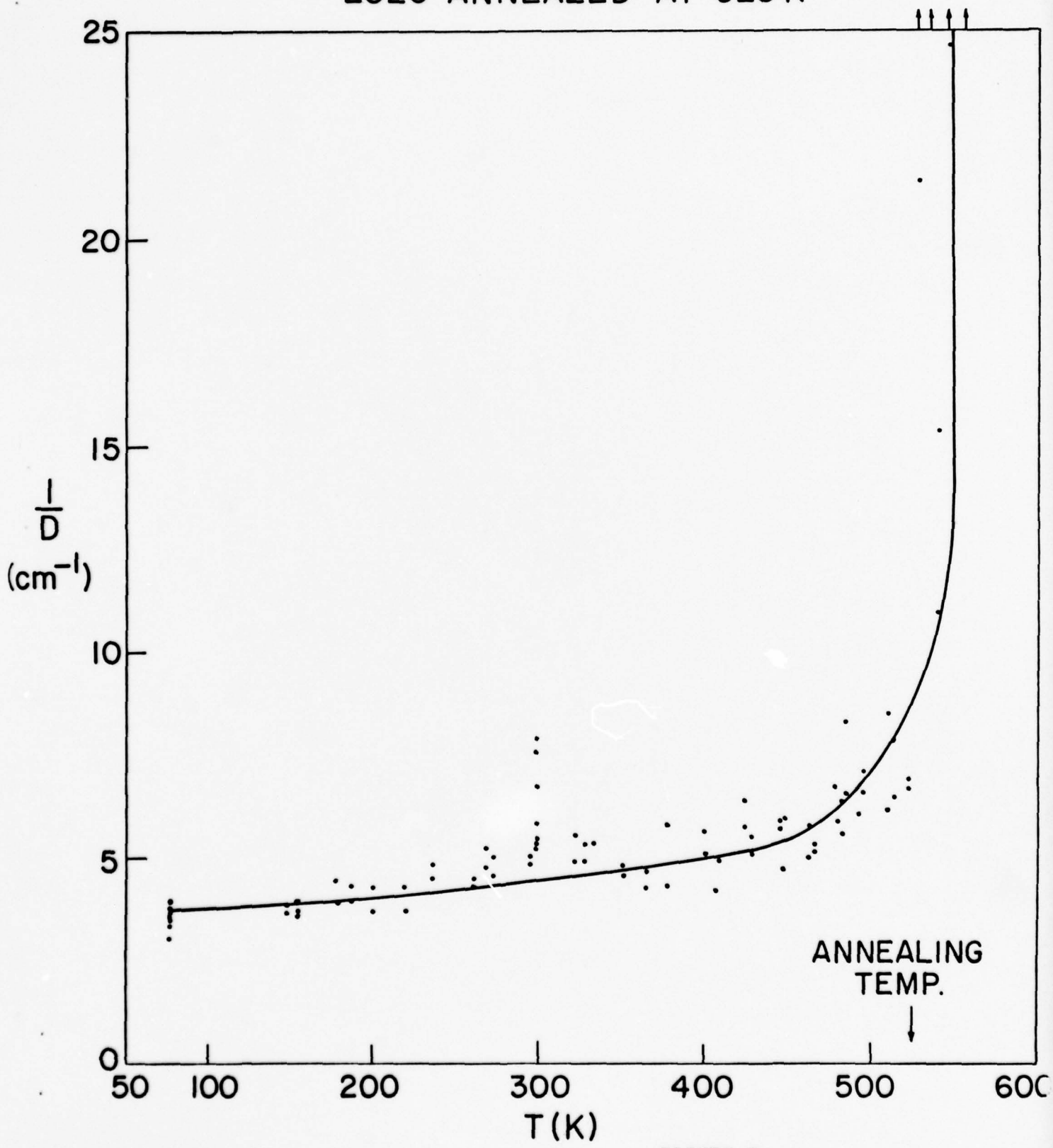
1/FRACTURE SEPARATION vs TEMPERATURE
2826 ANNEALED AT 523 K
25
20
15
10
5
0
1/D
(cm⁻¹)
50
100
200
300
400
500
600
T(K)
ANNEALING
TEMP.

FIGURE 8

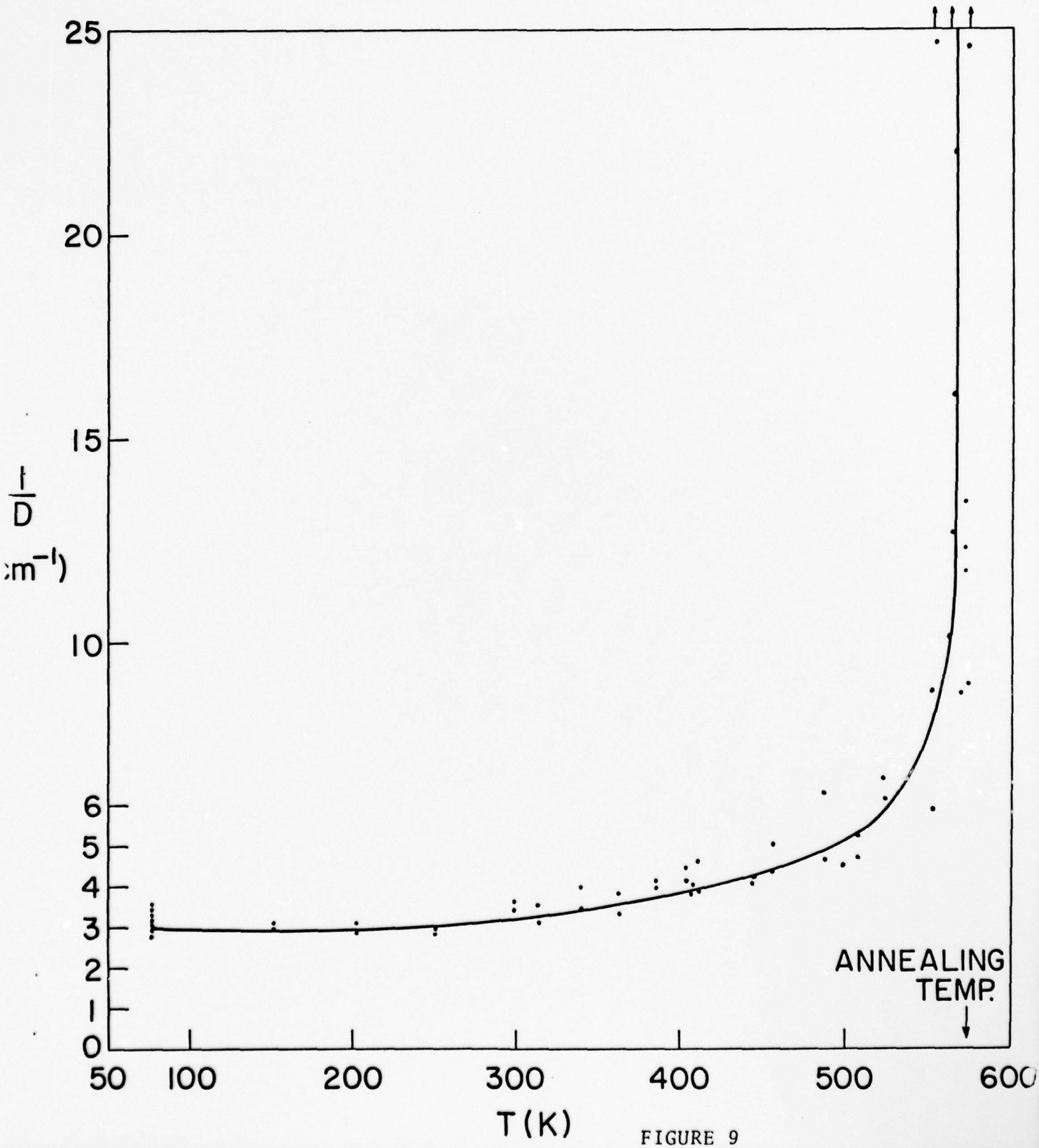
1/FRACTURE SEPARATION vs TEMPERATURE
2826 ANNEALED AT 573 K
25
20
15
10
6
5
4
3
2
1
0
1/D
(m⁻¹)
50
100
200
300
400
500
600
T(K)
ANNEALING TEMP.

FIGURE 9

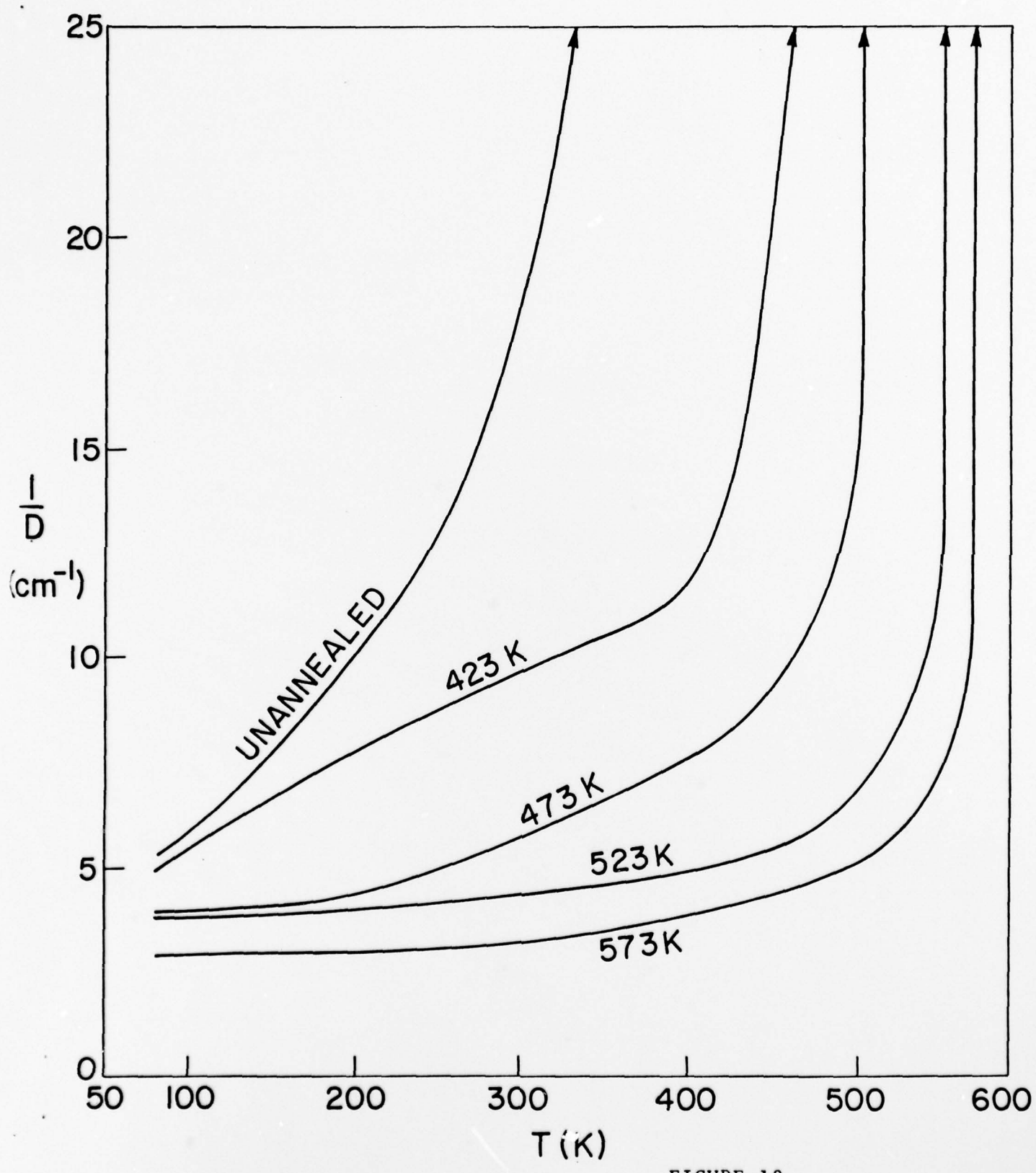
1/FRACTURE SEPARATION vs TEMPERATURE
25
20
15
10
5
0
1/D
(cm⁻¹)
UNANNEALED
423K
473K
523K
573K
50
100
200
300
400
500
600
T(K)

FIGURE 10

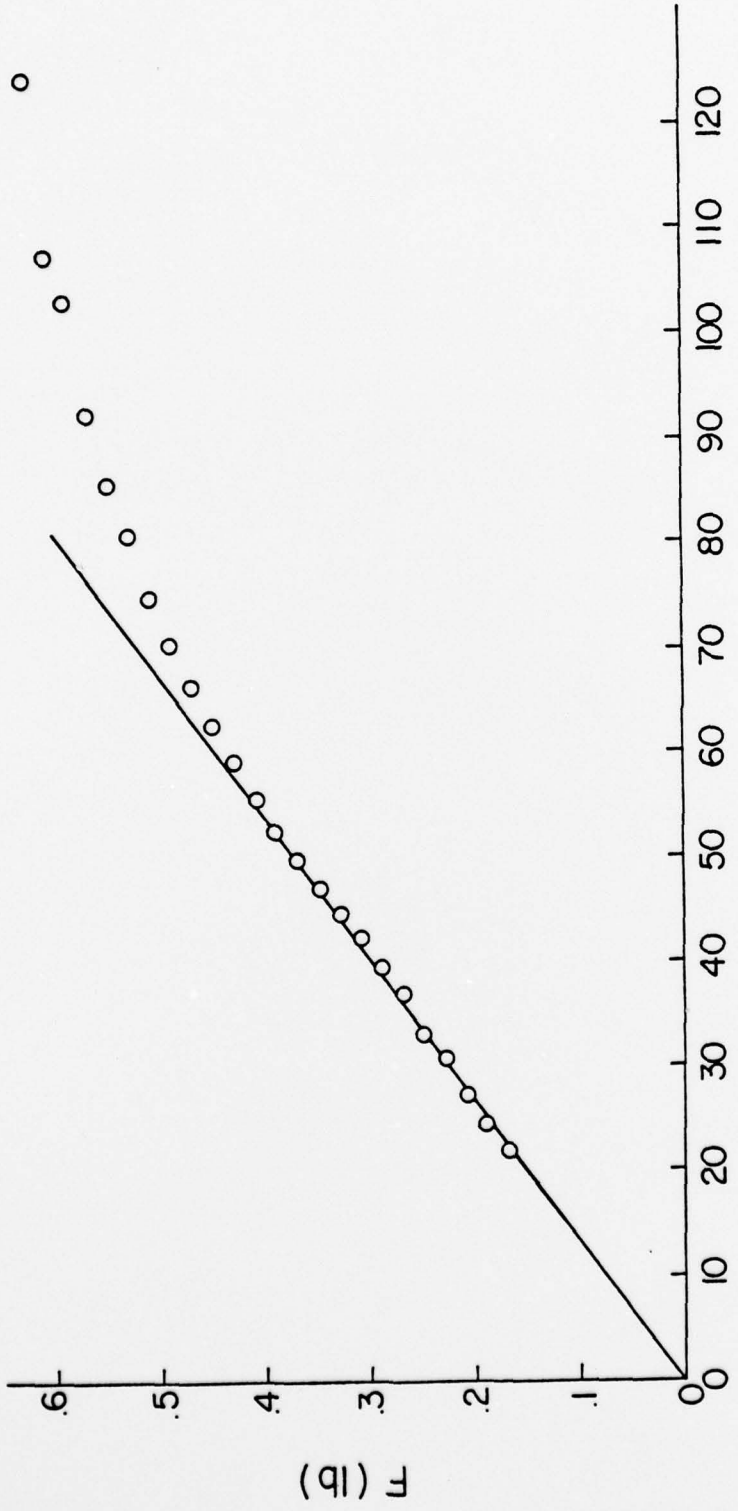

FIGURE 11

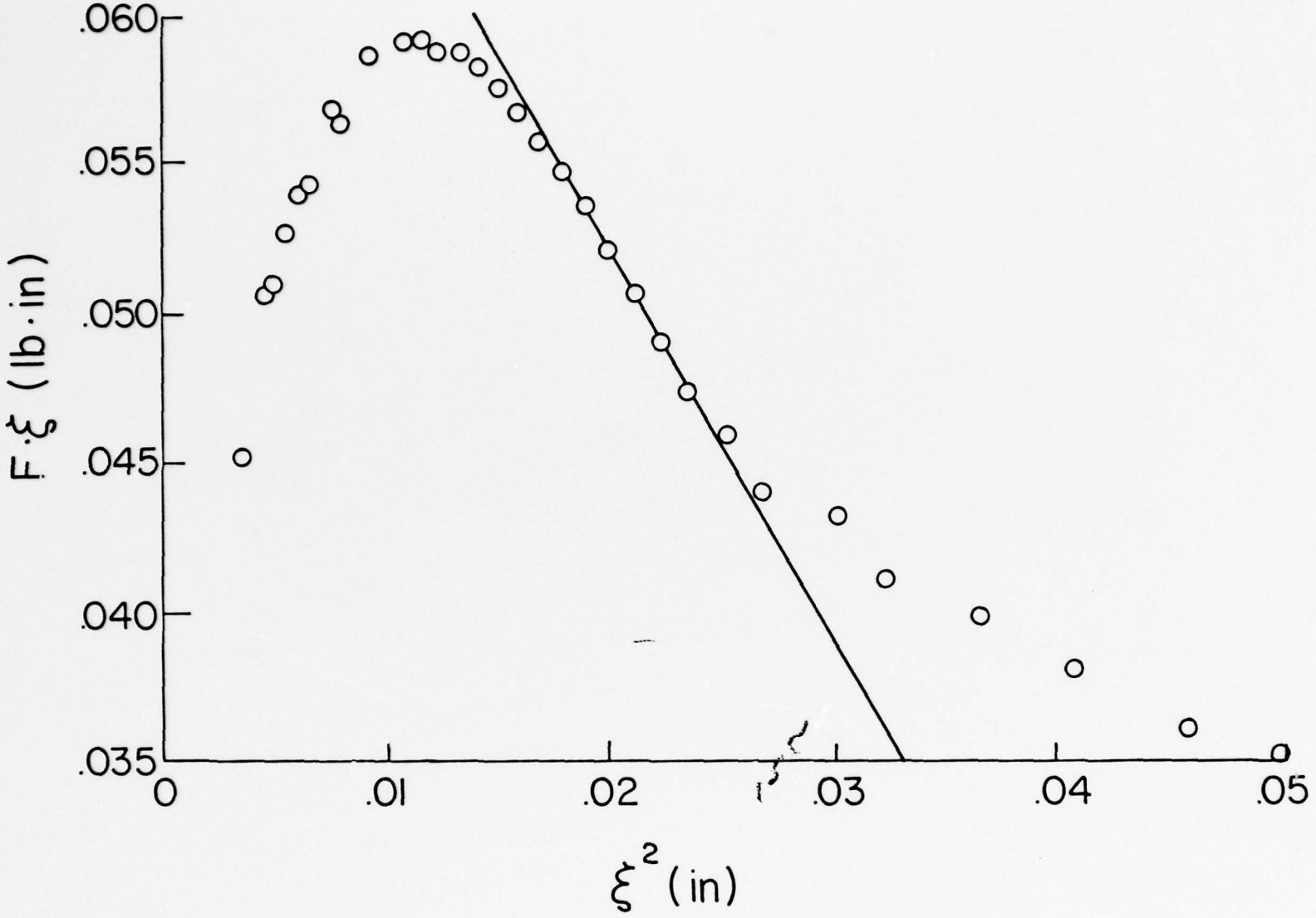

FIGURE 12

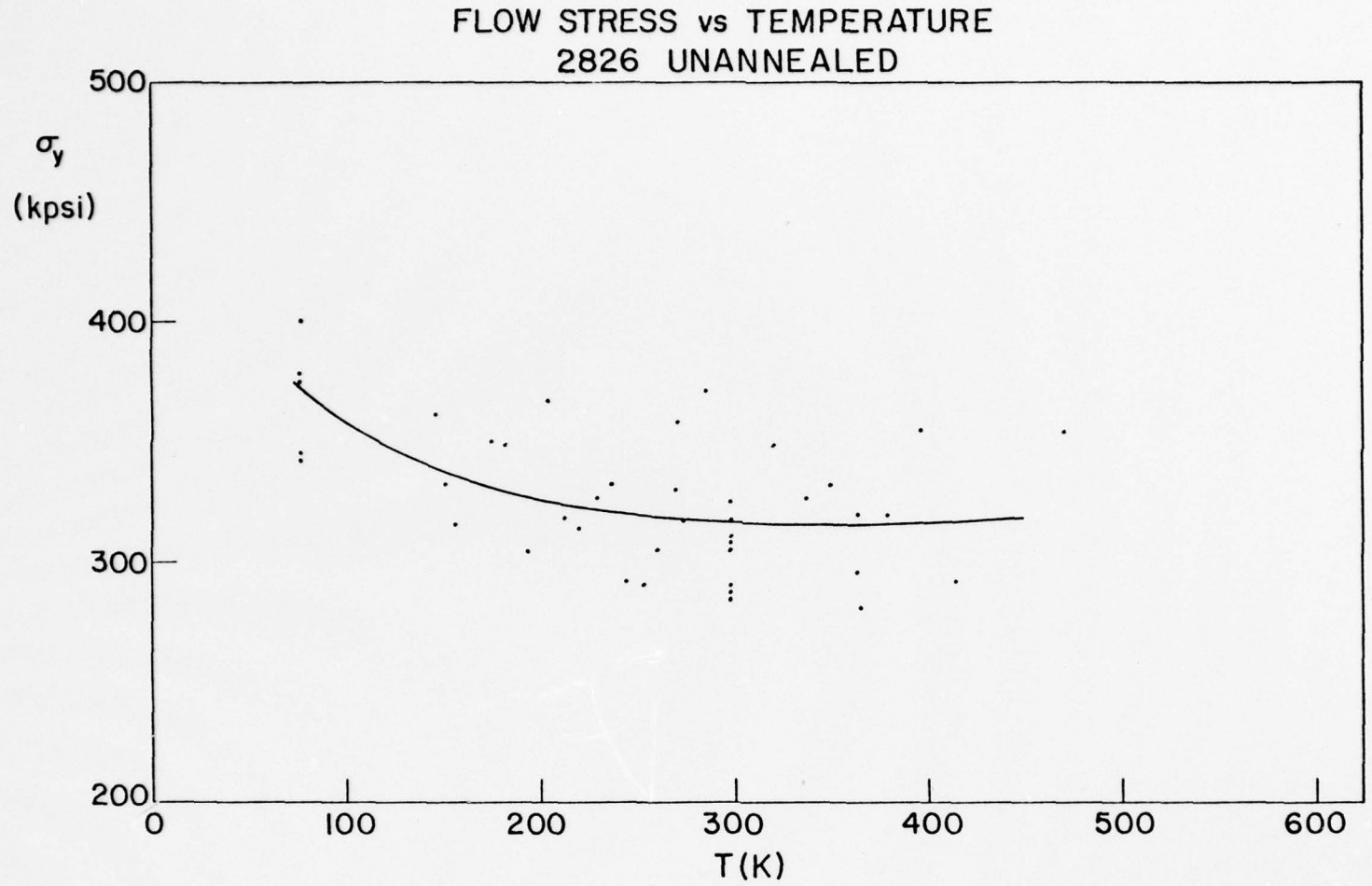
FLOW STRESS vs TEMPERATURE
2826 UNANNEALED
500
400
300
200
σ_y
(kpsi)
0
100
200
300
400
500
600
T(K)

FIGURE 13

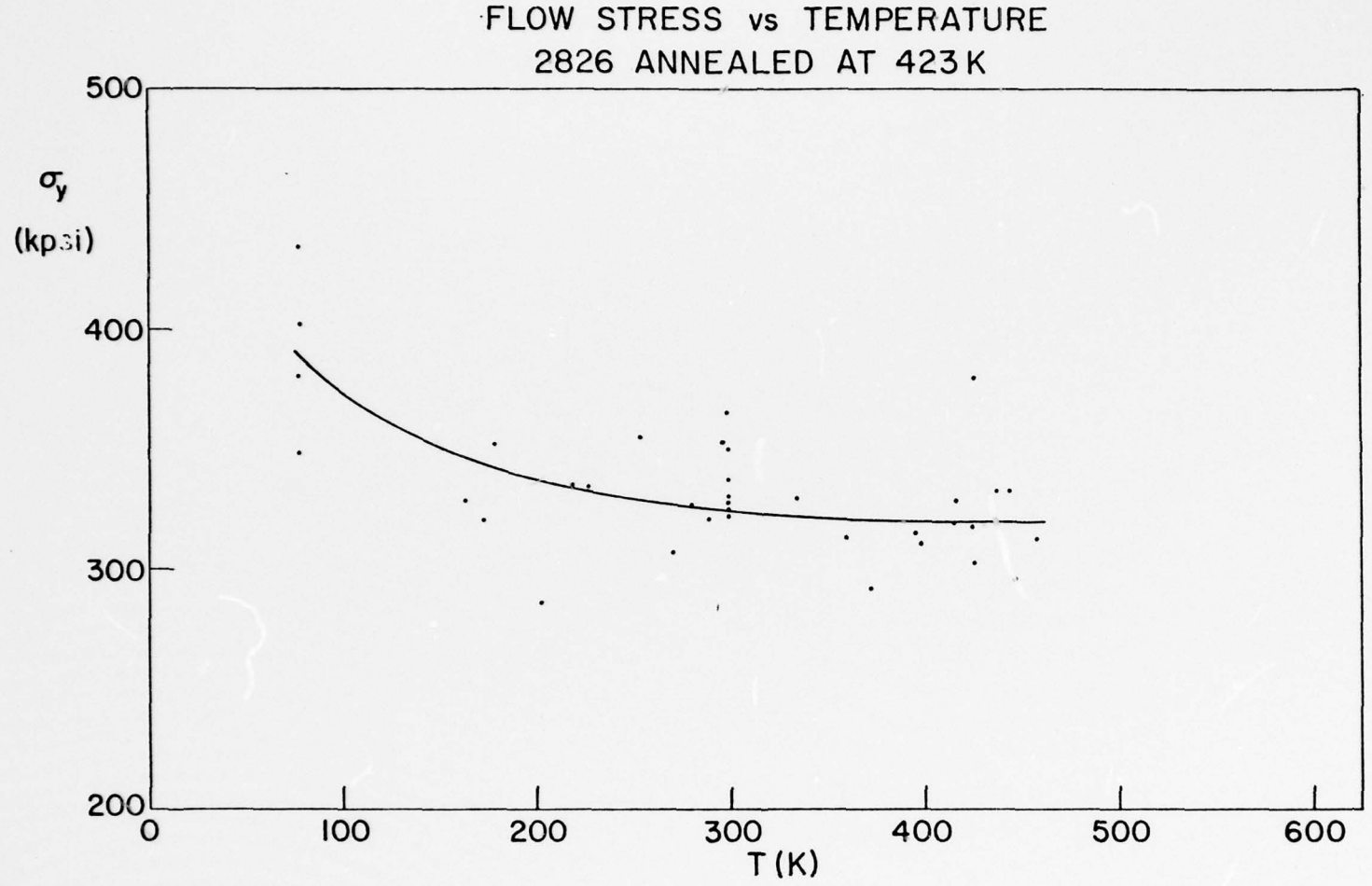
FLOW STRESS vs TEMPERATURE
2826 ANNEALED AT 423 K
500
400
300
200
σ_y
(kpsi)
0
100
200
300
400
500
600
T (K)

FIGURE 14

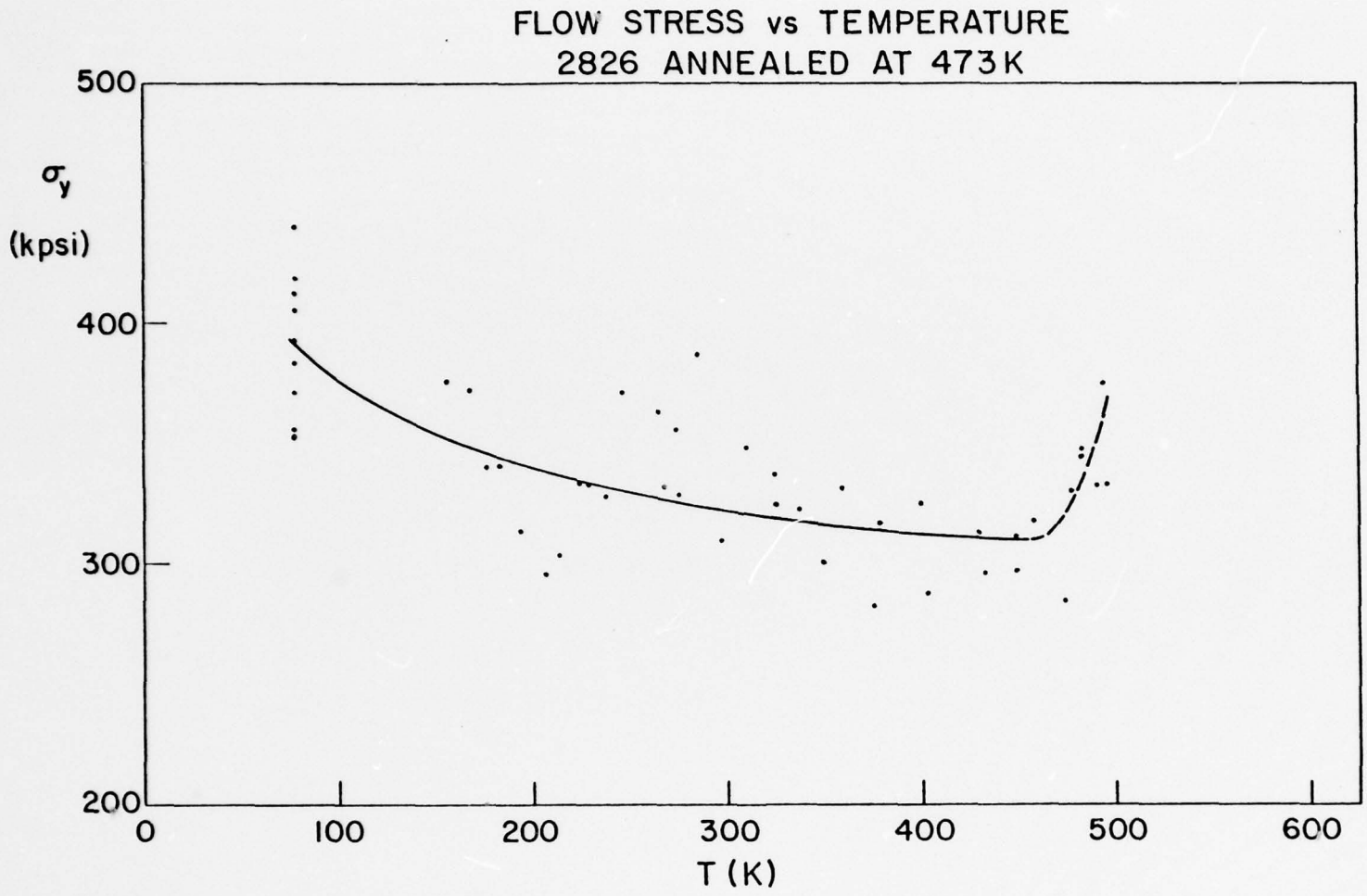
FLOW STRESS vs TEMPERATURE
2826 ANNEALED AT 473K
500
400
300
200
σ_y
(kpsi)
0
100
200
300
400
500
600
T (K)

FIGURE 15

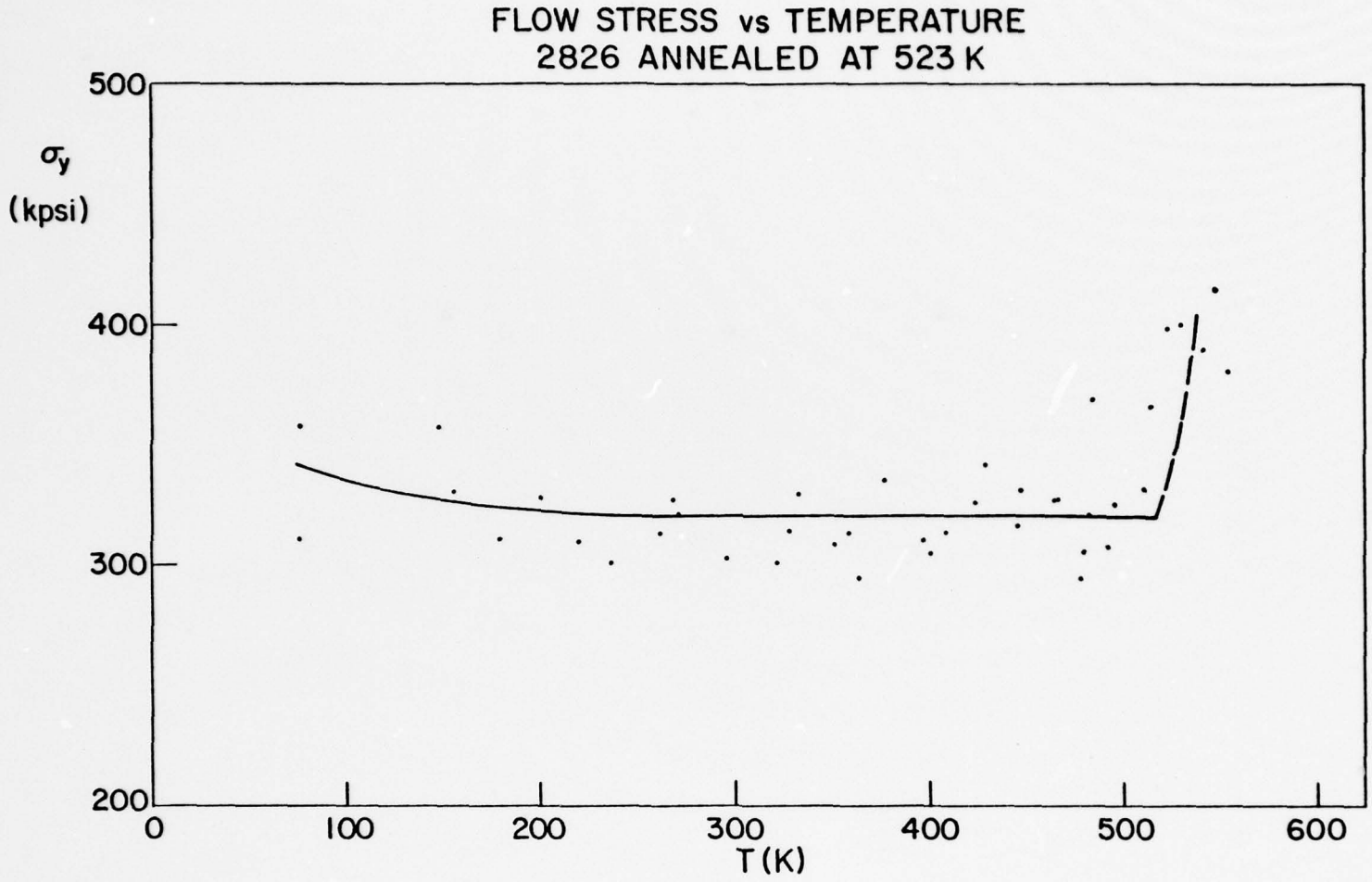
FLOW STRESS vs TEMPERATURE
2826 ANNEALED AT 523 K
500
400
300
200
σ_y
(kpsi)
0
100
200
300
400
500
600
T(K)

FIGURE 16

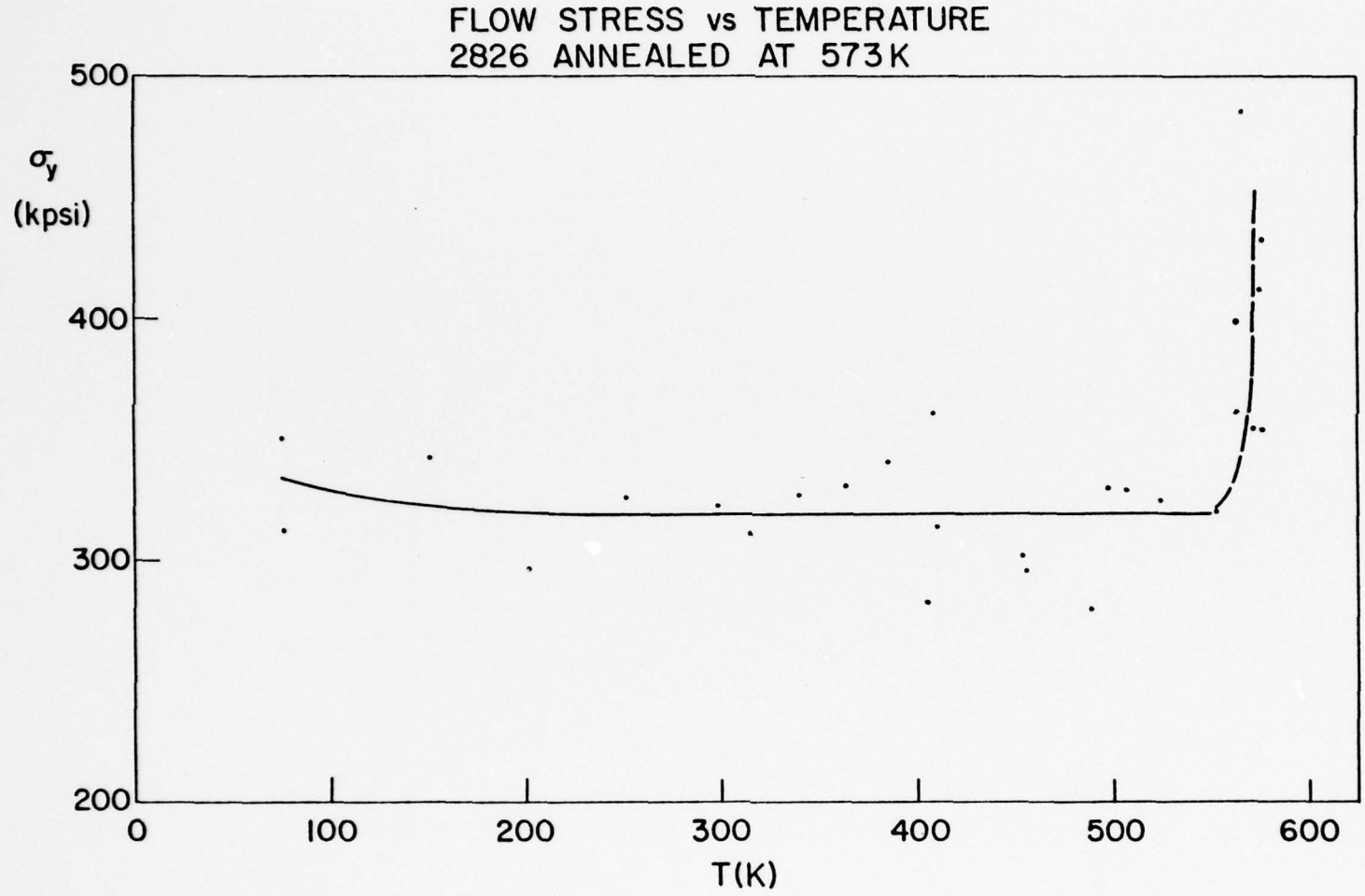
FLOW STRESS vs TEMPERATURE
2826 ANNEALED AT 573K
500
400
300
200
σ_y
(kpsi)
0
100
200
300
400
500
600
T(K)

FIGURE 17

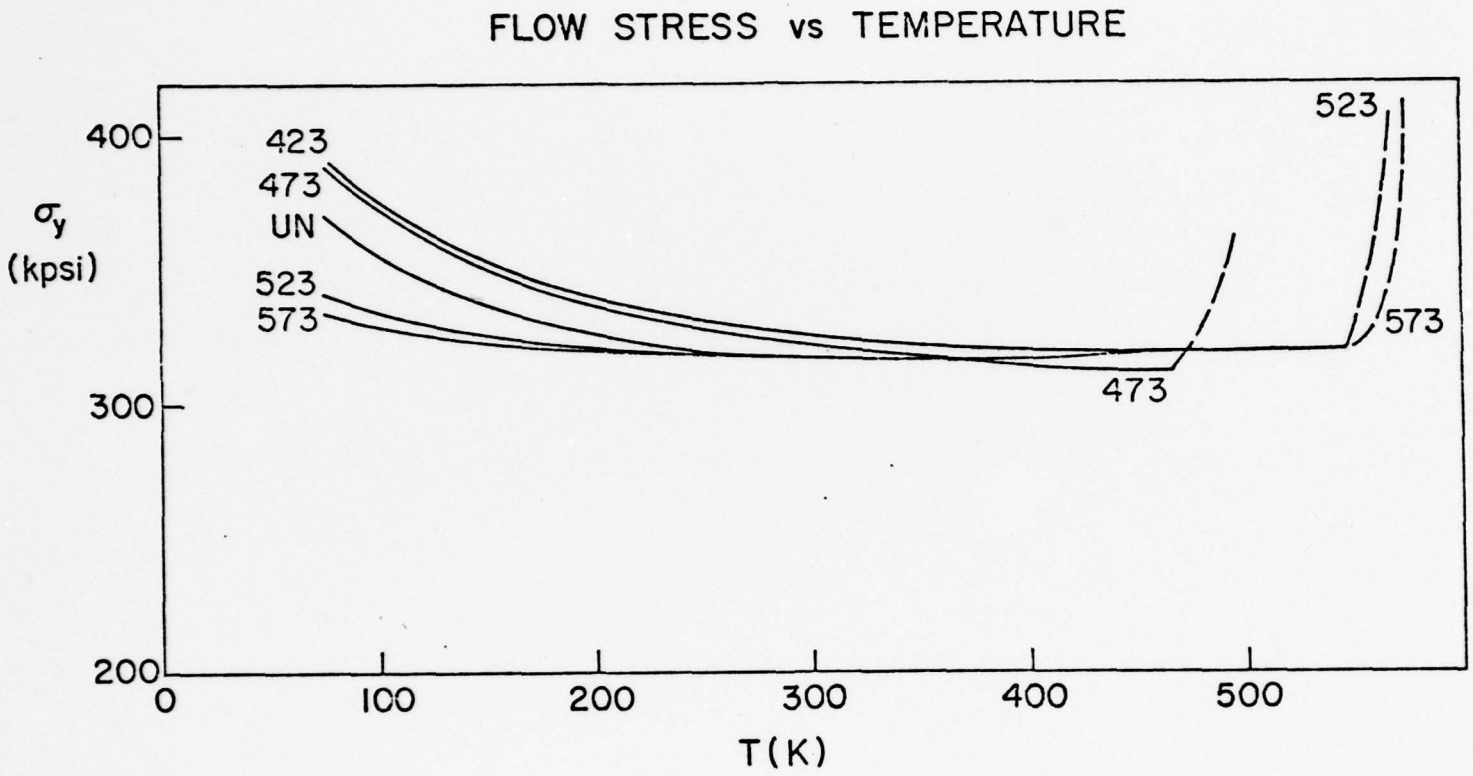
FLOW STRESS vs TEMPERATURE
400
300
200
σ_y
(kpsi)
423
473
UN
523
573
523
573
473
0
100
200
300
400
500
T(K)

FIGURE 18

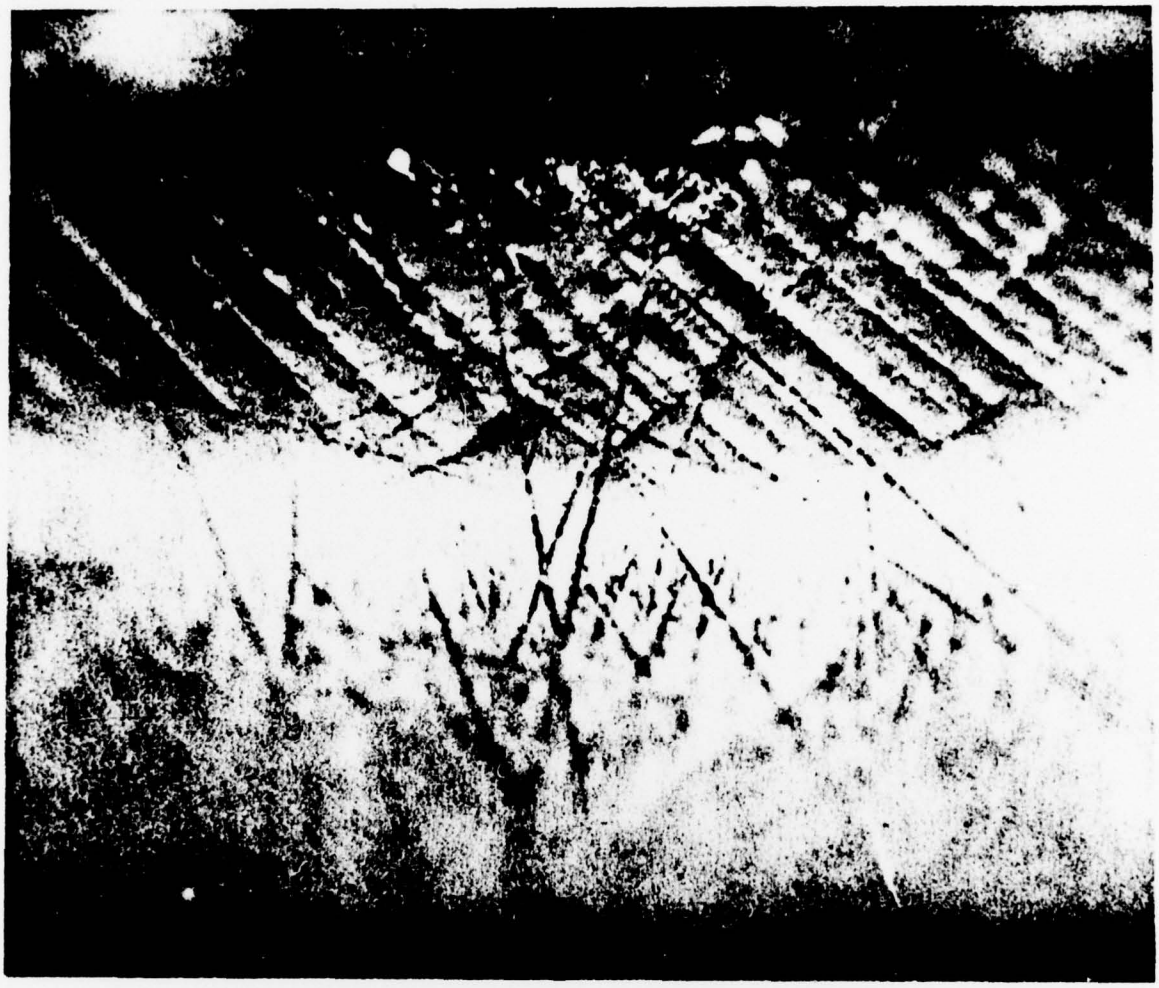

FIGURE 19

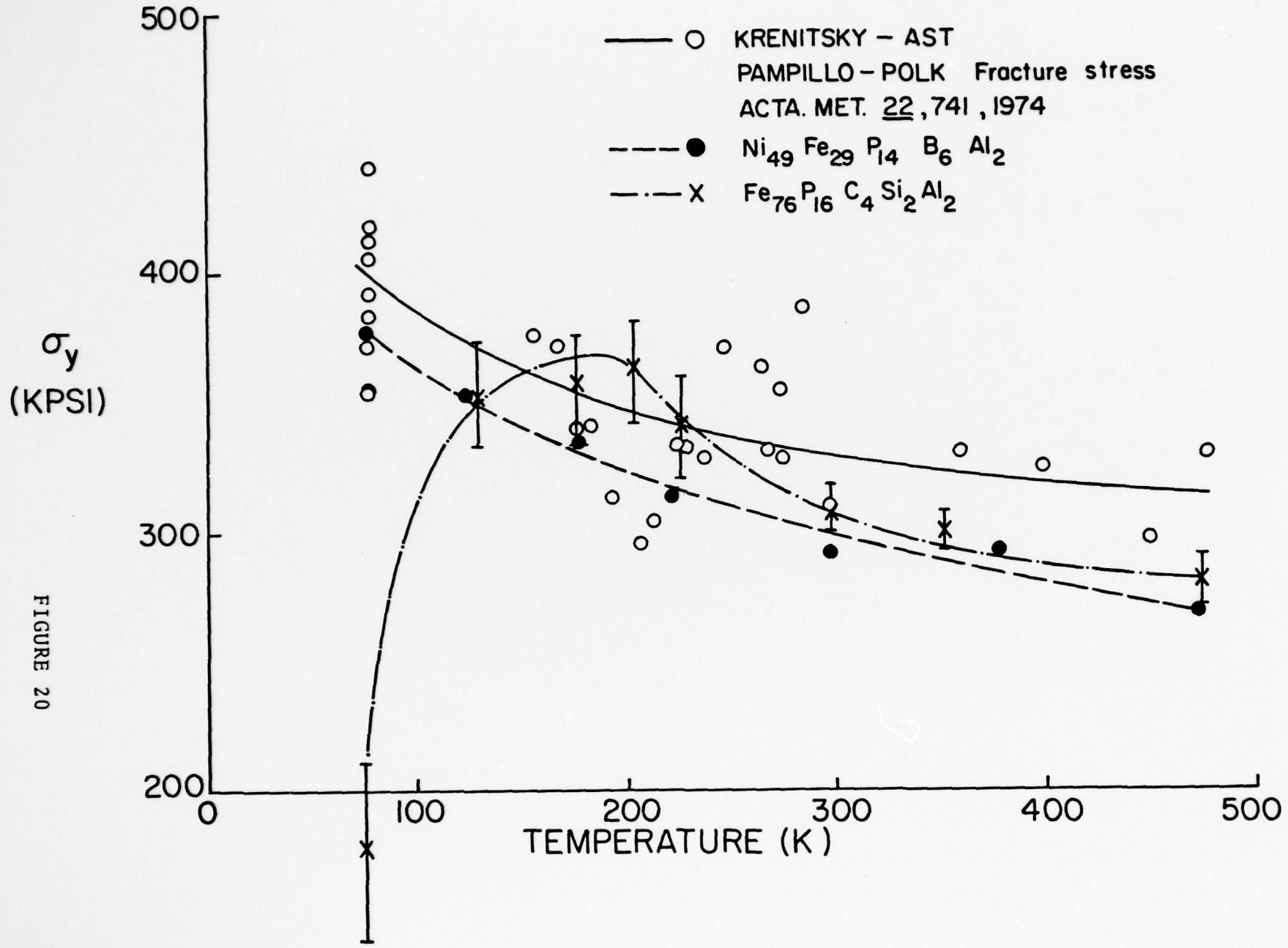
500
400
300
200
0
100
200
300
400
500
σ_y
(KPSI)
TEMPERATURE (K)
KRENITSKY – AST
PAMPILLO – POLK Fracture stress
ACTA. MET. 22, 741, 1974
$Ni_{49}\ Fe_{29}\ P_{14}\ B_6\ Al_2$
$Fe_{76}\ P_{16}\ C_4\ Si_2\ Al_2$

FIGURE 20

BASIC DISTRIBUTION LIST

Technical and Summary Reports April 1978

Organization	Copies
Defense Documentation Center Cameron Station Alexandria, VA 22314	12
Office of Naval Research Department of the Navy 800 N. Quincy Street Arlington, VA 22217	
ATTN: Code 471	1
Code 102	1
Code 470	1
Commanding Officer Office of Naval Research Branch Office Building 114, Section D 666 Summer Street Boston, MA 02210	1
Commanding Officer Office of Naval Research Branch Office 536 South Clark Street Chicago, IL 60605	1
Office of Naval Research One Hallidie Plaza Suite 601 San Francisco, CA 94102	1
Naval Research Laboratory Washington, DC 20375	
ATTN: Codes 6000	1
6100	1
6300	1
6400	1
2627	1
Naval Air Development Center Code 302 Warminster, PA 18964 ATTN: Mr. F. S. Williams	1

Organization	Copies
Naval Air Propulsion Test Center Trenton, NJ 08628 ATTN: Library	1
Naval Construction Batallion Civil Engineering Laboratory Port Hueneme, CA 93043 ATTN: Materials Division	1
Naval Electronics Laboratory San Diego, CA 92152 ATTN: Electron Materials Sciences Division	1
Naval Missile Center Materials Consultant Code 3312-1 Point Mugu, CA 92041	1
Commanding Officer Naval Surface Weapons Center White Oak Laboratory Silver Spring, MD 20910 ATTN: Library	1
David W. Taylor Naval Ship Research and Development Center Materials Department Annapolis, MD 21402	1
Naval Undersea Center San Diego, CA 92132 ATTN: Library	1
Naval Underwater System Center Newport, RI 02840 ATTN: Library	1
Naval Weapons Center China Lake, CA 93555 ATTN: Library	1
Naval Postgraduate School Monterey, CA 93940 ATTN: Mechanical Engineering Department	1

BASIC DISTRIBUTION LIST (cont'd)

Organization	Copies
Naval Air Systems Command Washington, DC 20360 ATTN: Codes 52031 52032	1
Naval Sea System Command Washington, DC 20362 ATTN: Code 035	1
Naval Facilities Engineering Command Alexandria, VA 22331 ATTN: Code 03	1
Scientific Advisor Commandant of the Marine Corps Washington, DC 20380 ATTN: Code AX	1
Naval Ship Engineering Center Department of the Navy Washington, DC 20360 ATTN: Code 6101	1
Army Research Office P.O. Box 12211 Triangle Park, NC 27709 ATTN: Metallurgy & Ceramics Program	1
Army Materials and Mechanics Research Center Watertown, MA 02172 ATTN: Research Programs Office	1
Air Force Office of Scientific Research Bldg. 410 Bolling Air Force Base Washington, DC 20332 ATTN: Chemical Science Directorate Electronics & Solid State Sciences Directorate	1 1
Air Force Materials Laboratory Wright-Patterson AFB Dayton, OH 45433	1
Library Building 50, Rm 134 Lawrence Radiation Laboratory Berkeley, CA	1

Organization	Copies
NASA Headquarters Washington, DC 20546 ATTN: Code RRM	1
NASA Lewis Research Center 21000 Brookpark Road Cleveland, OH 44135 ATTN: Library	1
National Bureau of Standards Washington, DC 20234 ATTN: Metallurgy Division Inorganic Materials Div.	1 1
Director Applied Physics Laboratory University of Washington 1013 Northeast Forthieth Street Seattle, WA 98105	1
Defense Metals and Ceramics Information Center Battelle Memorial Institute 505 King Avenue Columbus, OH 43201	1
Metals and Ceramics Division Oak Ridge National Laboratory P.O. Box X Oak Ridge, TN 37380	1
Los Alamos Scientific Laboratory P.O. Box 1663 Los Alamos, NM 87544 ATTN: Report Librarian	1
Argonne National Laboratory Metallurgy Division P.O. Box 229 Lemont, IL 60439	1
Brookhaven National Laboratory Technical Information Division Upton, Long Island New York 11973 ATTN: Research Library	1
Office of Naval Research Branch Office 1030 East Green Street Pasadena, CA 91106	1

SUPPLEMENTARY DISTRIBUTION LIST

Technical and Summary Reports November 1978

Professor G. S. Ansell
Rensselaer Polytechnic Institute
Department of Metallurgical
Engineering
Troy, NY 12181

Professor Dieter G. Ast
Cornell University
Department of Materials Science
and Engineering
Ithaca, NY 14853

Dr. E. M. Breinan
United Technologies Corporation
United Technologies Research Center
East Hartford, CT 06108

Professor H. D. Brody
University of Pittsburgh
School of Engineering
Pittsburgh, PA 14213

Dr. R. W. Cahn
University of Sussex
School of Engineering and
Applied Science
Brighton BN1 9QT
ENGLAND

Dr. E. A. Clark
Solid State Division
Naval Surface Weapons Center
White Oak Laboratory
Silver Spring, MD 20910

Dr. S. M. Copley
University of Southern California
Los Angeles, CA 90007

Professor M. Cohen
Massachusetts Institute of Technology
Department of Metallurgy
Cambridge, MA 02139

Dr. R. B. Diegle
Battelle
505 King Avenue
Columbus, OH 43201

Professor B. C. Giessen
Northeastern University
Department of Chemistry
Boston, MA 02115

Professor N. J. Grant
Massachusetts Institute of Technology
Department of Materials Science
and Engineering
Cambridge, MA 02100

Dr. F. E. Luborsky
General Electric Company
P. O. Box 8
Corporate R&D
Schenectady, NY 12301

Dr. J. Perel
Phrasor Technology
1536 Highland Avenue
Duarte, CA 91010

Professor O. D. Sherby
Stanford University
Materials Science Division
Stanford, CA 94300

Professor D. Turnbull
Harvard University
Division of Engineering and
Applied Physics
Cambridge, MA 02138

Professor R. Mehrabian
University of Illinois
Department of Mechanical and
Industrial Engineering
Urbana, IL 61801

Professor P. R. Strutt
University of Connecticut
School of Engineering
Department of Metallurgy
Storrs, CT 06268